

Nonlinearity-induced Band Gap Transmission in Dispersive and Flat Band Photonic Lattices

Avinash Tatarwal, Shailja Sharma, and Sebabrata Mukherjee*

Department of Physics, Indian Institute of Science, Bangalore 560012, India

(Dated: June 17, 2025)

Nonlinear interactions in photonic non-dispersive (flat) bands remain largely unexplored, despite their potential to yield exotic phenomena. Here, we demonstrate nonlinearity-induced transport of light from a boundary waveguide into photonic lattices with dispersive and flat bands. For the one-dimensional lattice supporting a dispersive band, self-focusing Kerr nonlinearity effectively makes the boundary waveguide phase-matched with the lattice modes, enabling efficient energy transfer above a threshold input power. In contrast, such nonlinear transmission to the flat band modes is inhibited, as demonstrated in a rhombic lattice supporting an isolated flat band. Instead, as the nonlinearity increases, light couples periodically to the lattice edge mode and then gradually spreads into the lattice due to the excitation of the lower dispersive band.

Periodic arrays of coupled optical waveguides provide a versatile platform for exploring how the transport of light is influenced by lattice geometry, synthetic gauge fields, disorder, and nonlinearity [1–6]. The lattice geometry, together with synthetic gauge fields, can determine the band dispersion – i.e., the variation of ‘energy’ with quasi-momentum – which influences the spreading or the diffraction of light in a lattice. On the other hand, nonlinearity can, in general, suppress diffraction, leading to the formation of shape-preserving nonlinear waves such as solitons [6–9] and discrete breathers [10–13].

In the context of wave transmission in a periodic medium, the presence of a band gap implies that certain states with energies within the gap can not propagate, effectively blocking the energy transmission. However, band gap transmission can be achieved by introducing nonlinearity in the system. Specifically, Ref. [14] proposed a discrete

* mukherjee@iisc.ac.in

sine-Gordon lattice driven at one end with energies within a band gap. For low-amplitude linear driving at the edge, no energy flows through the lattice; however, above a threshold nonlinear strength, sudden energy flow occurs due to the formation of nonlinear modes. This effect, coined as nonlinear supra-transmission, is a general wave phenomenon that can be observed in various setups, including nonlinear waveguide arrays [15–21]. Here, we investigate nonlinear band gap transmission using femtosecond laser-fabricated photonic lattices that are weakly coupled to a boundary waveguide with a relatively lower linear refractive index. In our experiments, intense laser pulses are coupled to the boundary waveguide, introducing self-focusing optical Kerr nonlinearity that causes an intensity-dependent increase in the refractive index. Unlike the supra-transmission models [15–19], the nonlinearity in our case effectively makes the boundary waveguide phase-matched with the lattice, enabling energy transfer to the lattice modes.

We then study nonlinear band gap transmission in a quasi-one-dimensional rhombic lattice supporting an isolated flat band. Compact localized flat band modes [22, 23] exhibit fascinating localization effects due to their infinite effective mass. While linear transport in flat-band photonic lattices [24–32] has been studied, nonlinear effects in such systems remain largely unexplored. Here, we experimentally and numerically show that the aforementioned nonlinear band gap transmission to the flat band modes does not occur. However, up to a certain nonlinear strength, periodic light transfer is observed to the lattice edge mode due to the formation of discrete breathers [10–13]. At higher nonlinearities, we demonstrate efficient light transfer to the lower dispersive band of the lattice.

In the scalar-paraxial approximation, light propagation through evanescently coupled waveguide networks can be described by the following discrete nonlinear Schrödinger equation [2, 3]:

$$i \frac{\partial}{\partial z} \psi_s(z) = \sum_{s'} H_{ss'}^{\text{lin}} \psi_{s'} - g |\psi_s|^2 \psi_s, \quad (1)$$

where z is the propagation distance, s labels the waveguides, $H_{ss'}^{\text{lin}}$ are the elements of the linear tight-binding Hamiltonian, and ψ_s is proportional to the slowly varying complex amplitude of the optical field at the s -th waveguide. The nonlinear parameter $g = 2\pi n_2 / (\lambda A_{\text{eff}})$ is determined by the nonlinear refractive index coefficient n_2 , the effective area of the waveguide modes A_{eff} , and the wavelength λ of light [33]. In the absence of

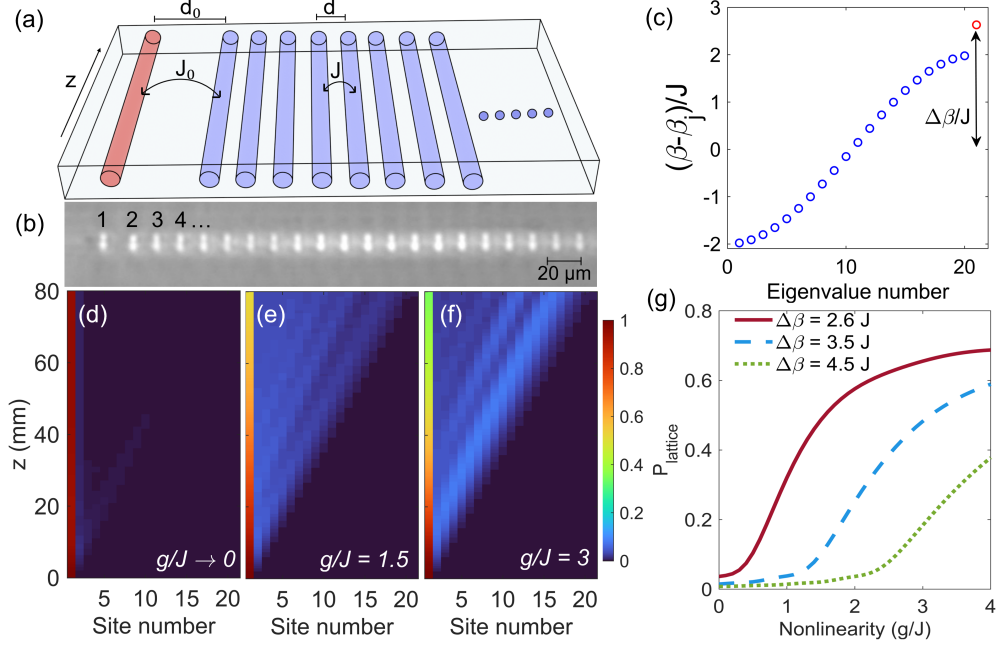


Figure 1. (a) Sketch of a one-dimensional array of identical waveguides, each with propagation constant β and coupling strength J . A boundary waveguide with a lower propagation constant $\beta_0 < \beta$ is weakly connected to the array with a smaller coupling $J_0 < J$. (b) Micrograph (cross-section) of the photonic device fabricated using femtosecond laser-writing. (c) Numerically calculated eigenvalue spectrum of the device, consisting of 20 sites in the lattice. The red circle corresponds to the boundary mode. Here, $\Delta\beta \equiv \beta - \beta_0 = 2.6J$, and $J_0 = 0.29J$. (d-f) Calculated light propagation through the device for three different nonlinear strengths g/J , with input excitation at the boundary waveguide. (g) Variation of power in the lattice P_{lattice} as a function of g/J for three different $\Delta\beta$. Nonlinearity causes light transmission to the lattice above a threshold nonlinearity of $g_{\text{th}} = \Delta\beta - 2J$ in each case.

optical losses, the total energy and the renormalized power ($P = \sum_s |\psi_s|^2$) are conserved. Note that the nonlinearity in the off-diagonal coupling terms is negligible in our experiments.

We first consider a one-dimensional photonic lattice consisting of N identical single-mode waveguides with nearest-neighbor coupling J . One end of the lattice is weakly coupled to a boundary waveguide, with coupling strength $J_0 < J$. This boundary waveguide has a lower propagation constant β_0 compared to the waveguides in the lattice, such that $\Delta\beta \equiv \beta - \beta_0 > 2J$. In Fig. 1(a), the lattice and the boundary sites are highlighted in blue

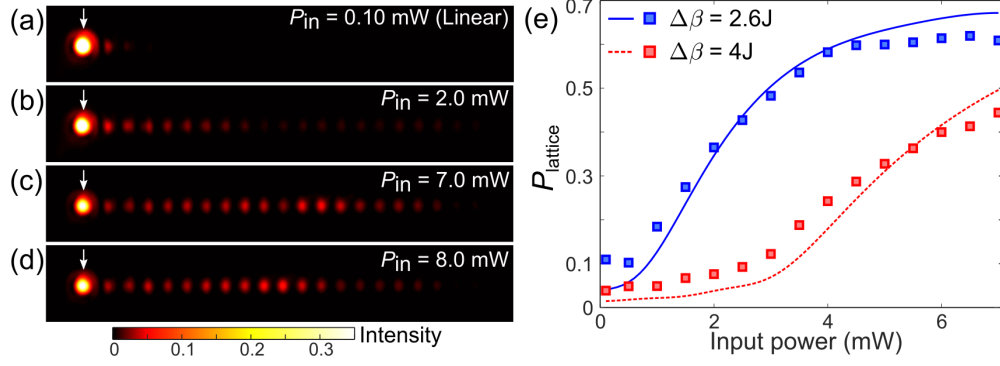


Figure 2. (a-d) Experimentally measured output intensity distributions at $z = 76.2$ mm for four different input powers, as indicated on each image. The white arrow marks the waveguide where light is initially launched. Above a threshold nonlinearity, light transmission in the lattice increases. (e) The measured variation of the normalized power P_{lattice} in the lattice as a function of input power for two different values of $\Delta\beta/J = \{2.6, 4\}$. The filled squares (lines) are obtained experimentally (numerically).

and red, respectively. Fig. 1(c) shows the spectrum of the device for the experimentally realized parameters, $J = 0.12 \text{ mm}^{-1}$, $J_0 = 0.29J$, and $\Delta\beta = 2.6J$. The propagation constant of the linear lattice modes β_j (where $j = 1, 2, \dots, N + 1$) spans from $\beta + 2J$ to $\beta - 2J$, while the boundary mode (red) lies in the upper band gap. Note that a small J_0 value ensures minimal impact of the boundary waveguide on the lattice spectrum. Figs. 1(d-f) show numerically calculated linear and nonlinear light propagation through the lattice over a propagation length of 80 mm. In the linear regime ($g \rightarrow 0$), the initial state coupled into the boundary waveguide remains mostly localized as shown in Fig. 1(d). Indeed, light transport from the boundary waveguide to the lattice is suppressed in the linear regime when $\Delta\beta > 2J$. However, the introduction of nonlinearity can enable transmission to the lattice, as shown in Figs. 1(e, f), for $g/J = 1.5$ and 3. Fig. 1(g) illustrates how the power transmitted to the lattice varies with the nonlinearity strength g/J for three different values of $\Delta\beta = 2.6J, 3.5J$ and $4.5J$. Notice the sharp increase in transmission above a threshold nonlinearity of $\Delta\beta - 2J$ in each case. It should be highlighted that similar nonlinearity-induced band gap transmission above a threshold nonlinearity occurs in supra-transmission models [15–19], where the boundary waveguide is essentially linear.

To demonstrate the above-mentioned nonlinear band gap transmission, we fabricate

optical devices in a 76.2 mm-long borosilicate glass (Corning Eagle-XG) substrate using the well-established technique of femtosecond laser-writing [34, 35]. The substrate is mounted on Aerotech x - y - z translation stages, and each waveguide is created by translating the substrate once through the focus of a 500 kHz train of 260 fs laser pulses generated by a fiber laser system (Satsuma, Amplitude). The fabrication parameters are optimized to inscribe well-confined, single-mode waveguides at an operational wavelength of 1030 nm. The evanescent coupling in the device is determined by the inter-waveguide spacing, and the relative propagation constant of the boundary waveguide is controlled by adjusting the translation speed of fabrication.

We fabricate 13 sets of photonic devices, as shown in Fig. 1(a, b), each with $d=16.5\ \mu\text{m}$ and $d_0=22\ \mu\text{m}$, where $\{d, d_0\}$ are the waveguide spacing in the lattice and the spacing from the boundary waveguide to the lattice, respectively. All $N=20$ waveguides in each lattice are inscribed at a translation speed of 6 mm/s, while the fabrication speed for the boundary waveguide is varied from 6 to 12 mm/s in steps of 0.5 mm/s. As discussed in the Supplemental document, the propagation constant detuning is calibrated as $\Delta\beta=0.085\Delta v$, where Δv is the difference in translation speed for fabricating the lattice and the boundary waveguide. For nonlinear experiments, we use the devices with the boundary site fabricated at $\{9.5, 11.5\}$ mm/s for which the value of $\Delta\beta$ is estimated to be $2.6J$ and $4J$, respectively.

To access self-focusing Kerr nonlinearity, we use temporally stretched, down-chirped 1.1 ps laser pulses with tunable pulse energy. For all transport experiments, we use horizontally polarized light at 1030 nm wavelength. Fig. 2(a) shows the measured output intensity distribution trapped at the boundary site in the linear regime. In this case, power transfer to the lattice is minimal – meaning, the boundary waveguide is effectively decoupled from the lattice due to its large propagation constant offset. As the nonlinearity is increased, we observe an increase in the total power in the lattice $P_{\text{lattice}} = \sum_{s=2}^{21} |\psi_s|^2 / \sum_{s=1}^{21} |\psi_s|^2$, as shown in Figs. 2(b-d). The variation of P_{lattice} with the average input power is shown in Fig. 2(e) (red data set). We perform similar experiments with a larger $\Delta\beta=4J$ and observe nonlinear band gap transmission with a relatively larger threshold power, as would be expected; see the blue data set in Fig. 2(e). The solid and dashed lines in this figure were obtained numerically (see Supplemental document). We note that these devices can be used as ultra-fast all-optical nonlinear switches [36–38] where the threshold input power can be adjusted by varying $\Delta\beta$. We also note that the

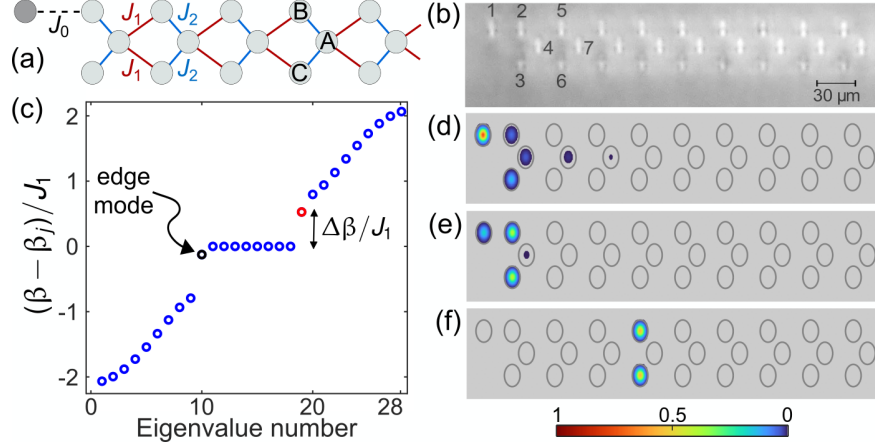


Figure 3. (a) Sketch of the photonic flat band rhombic lattice weakly coupled to a boundary waveguide with a propagation constant $\beta_0 < \beta$. (b) Transmission micrograph of the laser-fabricated photonic rhombic lattice. (c) Eigenvalue spectrum of the device, consisting of 28 sites. The lattice supports three bands – the upper and lower bands are dispersive, and the middle band is perfectly flat. Here, β_0 is adjusted such that the boundary mode (red) is detuned from the flat-band modes by Δ . Intensity distributions of the (d) boundary mode, (e) lattice edge mode and, (f) compact localized flat band mode.

maximum power transfer to the lattice can be enhanced beyond 95% by adjusting the system parameters such as the couplings, $\Delta\beta$, and propagation distance.

We now consider a quasi-one-dimensional rhombic array with three sites A, B, and C per unit cell. The inter- and intra-cell couplings are denoted by J_1 and J_2 , as shown in Fig. 3(a). In the nearest-neighbor tight-binding approximation, the lattice supports a perfectly flat band and two dispersive bands with eigenvalues

$$\begin{aligned} \epsilon_0(k) &= 0, \quad \text{and} \\ \epsilon_{\pm}(k) &= \pm \sqrt{2(J_1^2 + J_2^2 + 2J_1J_2 \cos(ka))}, \end{aligned} \quad (2)$$

respectively, where k is the quasi-momentum and a is the lattice constant. Unlike in previous experiments [26, 28], the bipartite nature of J_1 and J_2 makes the flat band isolated from the upper and lower dispersive bands. In our experiments, the lattice consists of $N = 27$ waveguides with $J_1 = 0.088 \text{ mm}^{-1}$ and $J_2 = 0.042 \text{ mm}^{-1}$. A boundary waveguide is weakly coupled to the B site at the end of the lattice, Fig. 3(a, b). The propagation constant difference of the boundary waveguide and its weak coupling to the lattice are $\Delta\beta = 0.42J_1$

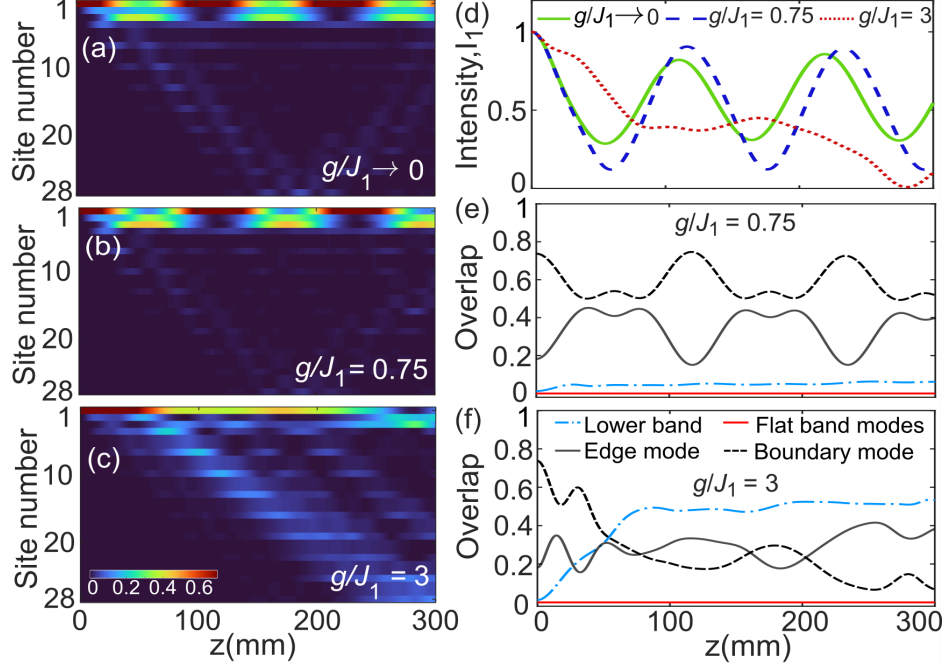


Figure 4. (a-c) Numerically calculated light propagation through the rhombic lattice for three different nonlinear strengths g/J_1 , as indicated on each image. (d) Variation of intensity in the boundary waveguide as a function of propagation distance. (e, f) Overlap of the normalized optical state with different eigenmodes of the system for two different g/J_1 values.

and $J_0 = 0.37J_1$, respectively. Fig. 3(c) shows the real-space spectrum of the device calculated using the experimentally realized parameters. The intensity distributions of the boundary mode, lattice edge mode, and a compact localized flat band mode are shown in Fig. 3(d-f), respectively. The flat band modes are localized to the B and C sites of a unit cell with equal intensity and opposite phases. The boundary mode spectrally resides in the gap above the flat band, whereas the lattice edge mode appears just below the flat band. Note that the boundary mode does not spatially overlap with the localized flat band modes.

To explore nonlinearity-induced transport from the boundary waveguide to the flat band lattice, we numerically calculate light propagation for three different g/J_1 values. In the linear regime, an input state localized at the boundary waveguide overlaps primarily with the lattice edge mode. As a result, a beating motion of intensity is observed with a partial transfer of light from the boundary to the B and C sites on the edge; see Figs. 4(a, d). As the nonlinear strength is increased, a similar beating motion of intensity is observed with a longer period and increased energy transfer to the lattice edge mode; see Figs. 4(b, d). Specifically,

for $g/J_1 \lesssim 1.2$, the z -periodic oscillation of optical intensity occurs due to the formation of discrete breathers on the edge of the lattice. We note that the discrete breathers are z -periodic localized nonlinear states which are distinct from shape-preserving spatial solitons. When the nonlinearity is further increased, modes of the lower dispersive band are excited; hence, we observe light transport to the lattice; Figs. 4(c, d). Evidently, nonlinearity causes efficient transfer of light to the lattice edge mode and to the lower dispersive band, but the flat band modes of the lattice are not excited. To further investigate, we calculate the overlap of the normalized optical state with different eigenmodes of the flat band system for two different $g/J_1 = 0.75$ and 3, as presented in Figs. 4(e, f). At low nonlinearity, the oscillating nature of the overlap with the lattice edge mode and the boundary mode indicates the periodic exchange of optical power between them. This behaviour is destroyed in Fig. 4(f), where the overlap with the lower band is significant. Importantly, notice that the total overlap with the flat band modes (solid red line) remains zero irrespective of the g/J_1 value. The light transfer to the flat band modes is inhibited because of the unique phase and intensity profiles of the flat band modes, which make their overlap with the boundary mode zero. In other words, the coupling between the boundary mode and the flat band modes remains zero irrespective of their propagation constant mismatch.

To demonstrate the signature of the nonlinear phenomena in Fig. 4, we launch laser pulses at the boundary site of the rhombic lattice and probe the intensity patterns at $z = 76.2$ mm. Figs. 5(a-c) show the measured intensity distributions for three different average input powers, as indicated on each figure. In the linear regime, most of the light stays in the boundary waveguide and in the edge sites of the lattice; see Fig. 5(a). Up to $P_{\text{in}} = 1.5$ mW, no significant spreading of light into the lattice is observed. However, notice the increased transfer of light from the boundary to the edge waveguides in Fig. 5(b), indicating the formation of nonlinear breathers. On the other hand, the spreading of light into the lattice is clearly visible in Fig. 5(c) – here, nonlinearity causes the excitation of modes of the lower dispersive band. To further clarify, we calculate and measure the light in the bulk of the lattice $P_{\text{bulk}} = \sum_{s=5}^{28} |\psi_s|^2 / \sum_{s=1}^{28} |\psi_s|^2$. Notice that P_{bulk} increases only after a threshold nonlinearity, when the lower dispersive band is excited, Fig. 5(d, h). At strong nonlinearities ($g/J_1 \gtrsim 2.5$), the nonlinear refractive index detuning at the boundary waveguide becomes large enough to suppress power transmission through the lattice, leading to a peak in P_{bulk} as a function of g/J_1 . We notice some deviation and asymmetry in our experiments due

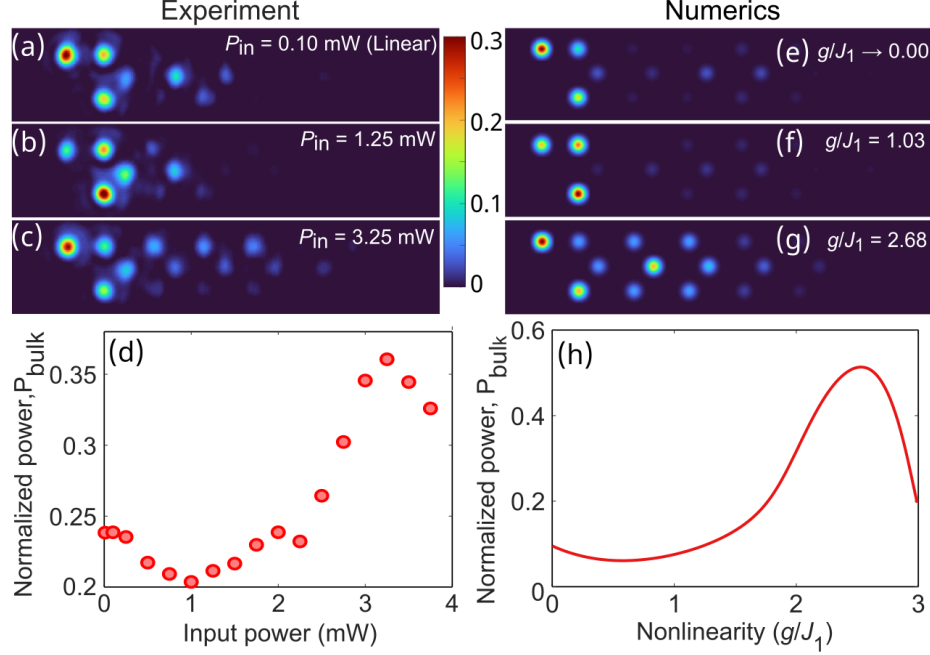


Figure 5. (a-c) Experimentally measured normalized intensity at $z = 76.2$ mm for three different values of P_{in} . The input power is indicated on each image. (e-g) Numerically calculated output intensity distributions associated with (a-c). (d, h) Measured and calculated variation of the power transmitted into the bulk of the lattice P_{bulk} as a function of the nonlinear strength.

to unavoidable random disorder and possible fabrication errors. That said, Fig. 5(a-d) qualitatively agrees with the numerical results in Fig. 5(e-h).

In summary, we have numerically and experimentally studied nonlinearity-induced band gap transmission from a boundary waveguide to photonic lattices. When the linear propagation constant of the boundary waveguide is in the band gap, light transfer to a one-dimensional lattice is possible above a threshold nonlinear strength. This work can find future applications in ultra-fast all-optical nonlinear switching and signal processing. In the case of a flat band rhombic lattice, we show that the nonlinearity can not couple light from the boundary waveguide to the flat band modes. We have observed periodic light transfer to the edge mode, and, subsequently, to the lower dispersive band of the lattice. For weak coupling J_0 to the lattice and short propagation distances (i.e., when the power depletion at the boundary site is not significant), optical nonlinearity can be used to selectively excite modes of a dispersive band. Evidently, photonic lattices provide a natural platform for exploring nonlinear interactions in flat bands, where such interactions can be

enhanced, opening new avenues for research [39–43]. Furthermore, our results will be useful to the fundamental science of discrete solitons and breathers.

Funding.— STARS, Ministry of Education, Government of India (MoESTARS/STARS-2/2023-0716); Indian Institute of Science (Start-up grant, IoE postdoctoral fellowship); Infosys Foundation, Bangalore; Council of Scientific & Industrial Research (PhD Scholarship).

Acknowledgments.— We sincerely thank Nicholas Smith of Corning Inc. for providing high-quality glass wafers used in the experiments.

Disclosures.— The authors declare no conflicts of interest.

Data Availability.— The data that support the findings of this study are available from the corresponding author upon reasonable request.

SUPPLEMENTARY DOCUMENT

A. BAND STRUCTURE OF THE FLAT BAND LATTICE

Light transport in our photonic lattices can be approximated by the coupled-mode equations. In this case, the Fourier-transformed Hamiltonian in k -space is expressed as the following 3×3 matrix

$$\mathcal{H} = - \begin{bmatrix} \beta_a & (J_1 + J_2 e^{ika}) & (J_1 + J_2 e^{ika}) \\ (J_1 + J_2 e^{-ika}) & \beta_b & 0 \\ (J_1 + J_2 e^{-ika}) & 0 & \beta_c \end{bmatrix} \quad (\text{A1})$$

where $J_{1,2}$ are the inter-waveguide couplings described in the main text and β_{a-c} are the propagation constants of A, B, and C sites of the unit cell. Since, all the waveguides in the rhombic lattice (not the boundary site) are fabricated using identical parameters, we consider $\beta_a = \beta_b = \beta_c = \beta$. In this situation, by diagonalizing the Fourier-transformed Hamiltonian, we obtain the eigenvalues as 0 and $\pm \sqrt{2(J_1^2 + J_2^2 + 2J_1 J_2 \cos(ka))}$ for the flat band and two dispersive bands, respectively.

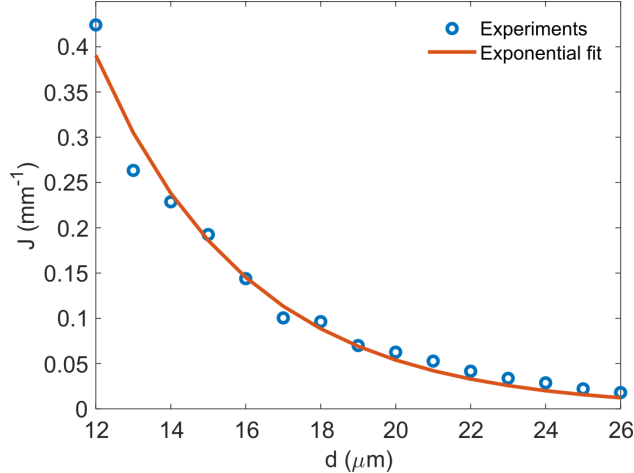


Figure 6. Variation of coupling strengths at 1030 nm wavelength with waveguide-to-waveguide separation d .

B. MEASUREMENT OF COUPLING STRENGTH

To investigate the variation of coupling strength J with the inter-waveguide separation d , we fabricated fifteen sets of directional couplers consisting of horizontally-coupled two straight waveguides. The separation d was systematically varied from 12 μm to 26 μm in steps of 1 μm . The measured variation of $J(d)$ is presented in Fig. 6. Evidently, the coupling strength decays exponentially with inter-waveguide spacing, as would be expected. Using Fig. 6 as a reference, we fabricated three sets of identical couplers with specific d -values, and the average coupling strengths are mentioned in the main text. We performed similar experiments to obtain couplings along the diagonal direction in the case of rhombic lattices.

C. CALIBRATION OF $\Delta\beta$

As described in the main text, we fabricated 13 sets of photonic devices, as shown in Fig. 1(a, b), varying the propagation constant shift $\Delta\beta$ of the boundary site. In experiments, $\Delta\beta = \beta - \beta_0$ is increased by fabricating the boundary waveguide at a higher translation speed. We couple low-power light at the boundary waveguide of each device and measure the output intensity distributions at $z = 76.2$ mm. For the device with $\Delta\beta = 0$, around 80% of light transmits to the lattice. As the propagation constant of the boundary waveguide

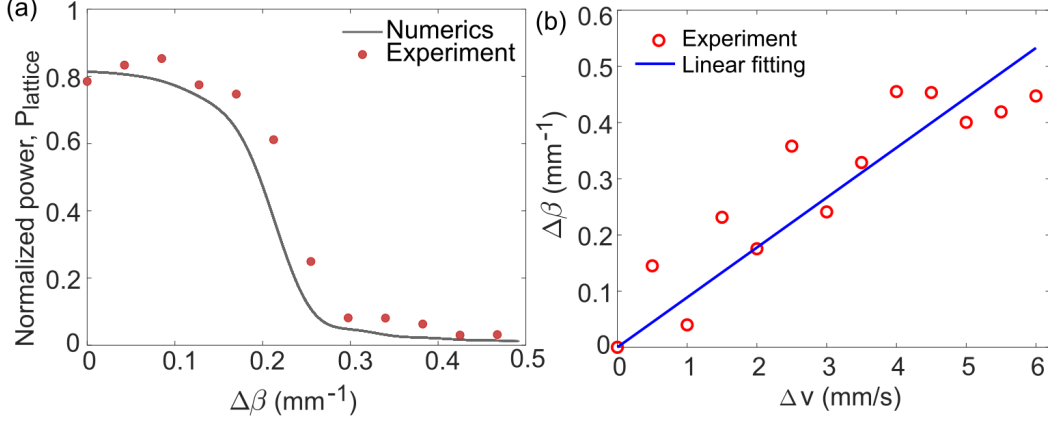


Figure 7. (a) The normalized intensity in the lattice as a function of $\Delta\beta$, which is experimentally tuned by varying the translation speed. (b) The variation of $\Delta\beta$ as a function of the change in fabrication speed. The red circles are the measured values of $\Delta\beta$, and the solid blue line is a linear fit.

is decreased by increasing its fabrication speed, power transmission in the lattice P_{lattice} decreases. The variation of P_{lattice} with translation speed is shown in Fig. 7(a). From this variation of P_{lattice} with translation speed, we calibrate the propagation constant detuning as $\Delta\beta = 0.085\Delta v$, where Δv is the difference in translation speed for fabricating the lattice and the boundary waveguide. The solid line in Fig. 7 (a) was calculated numerically by solving the coupled-mode Eq.1 in the linear regime ($g \rightarrow 0$).

In addition to the above approach, we calibrate $\Delta\beta$ by characterizing asymmetric directional couplers. To measure $\Delta\beta$ with translation speed, thirteen sets of isolated straight waveguide couplers (translation speeds 6 to 12 mm/s in steps of 0.5 mm/s) were fabricated. We injected low-power light beam in one of the waveguides (WG-1) of the coupler and measured the output intensity distribution.

We note that the output intensity distribution in an asymmetric coupler is given by

$$|\psi_1(z)|^2 = 1 - \frac{J^2}{\frac{1}{4}(\Delta\beta)^2 + J^2} \sin^2 \left[\left\{ \left(\frac{1}{4}(\Delta\beta)^2 + J^2 \right)^{\frac{1}{2}} z \right\} \right] \quad (\text{A2})$$

$$|\psi_2(z)|^2 = 1 - |\psi_1(z)|^2 \quad (\text{A3})$$

For our laser-written couplers with known coupling strength J , propagation distance z and output intensities $|\psi_{1,2}(z)|^2$, we can estimate $\Delta\beta$ as a function of Δv , see Fig. 7(b). This second approach gives a very similar calibration of propagation constant shift, $\Delta\beta = 0.088\Delta v$.

D. LOSS MEASUREMENT

The propagation loss of the laser-written waveguides is measured using the cut-back method. The insertion loss (arising due to propagation, coupling and Fresnel reflection losses) is measured for waveguides with two different lengths, i.e., 76.2 mm and 20 mm. From the difference in the insertion losses for the waveguides with these two different lengths, we obtain propagation loss coefficient, $\alpha \approx 0.04 \text{ cm}^{-1}$.

For all nonlinear experiments, we monitor both input and output power. The output power is found to vary linearly with the input power in our experiments. This observation indicates that the nonlinear loss due to multi-photon absorption can be neglected.

E. CALIBRATION OF NONLINEAR STRENGTH

To estimate how the nonlinear strength at the input, $g(z=0)$, varies as a function of average input power P_{in} , we probe the nonlinear dynamics in devices shown in Fig. 1(a). The light beam is coupled into the boundary waveguide of the device, and the normalized power in the lattice $P_{\text{lattice}}(z=76.2 \text{ mm})$ is measured as a function of the input power. The experimentally measured data for $\Delta\beta/J = \{2.6, 4\}$ in Figs. 2(e) are fitted with numerically calculated results by varying $g(0)$ as a free parameter. For both devices with two different values of Δ , we obtain $g(z=0) = 0.072 P_{\text{in}} \text{ mm}^{-1} \text{ mW}^{-1}$.

F. BOUNDARY WAVEGUIDE COUPLED TO THE EDGE A SITE

In the main text, we have numerically and experimentally studied the nonlinearity-induced transport of light from a boundary waveguide to the rhombic lattice. In that case, the boundary waveguide was coupled to the edge B site simply because the flat band modes are localized on the B and C sites of a unit cell. In this section, we numerically examine the case where the boundary waveguide is coupled to the edge A site as shown in the inset of Fig. 8(a).

We consider experimentally realized parameters as discussed in the main text. The eigenvalue spectrum of the device, consisting of 28 sites, is shown in Fig. 8(a). Unlike, Fig. 3(a) in the main text, there is no lattice edge mode in the band gap. When light is coupled to the boundary site, it remains strongly localized in the linear regime. At weak

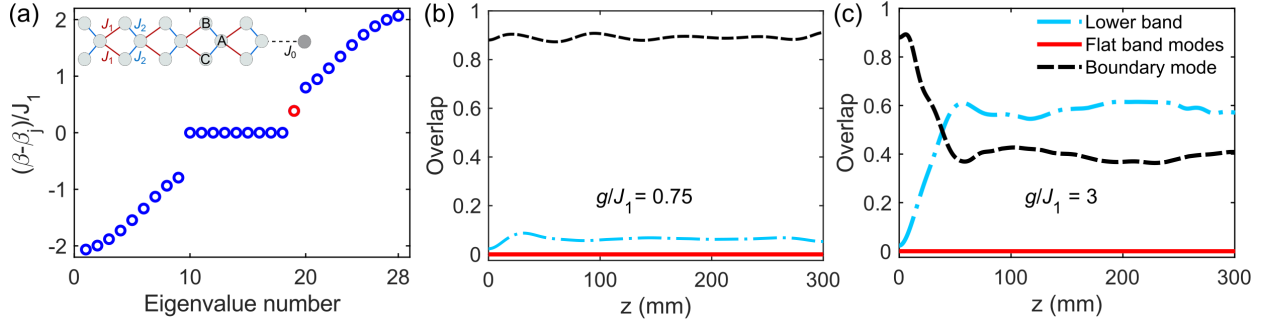


Figure 8. (a) Numerically calculated eigenvalue spectrum of the device, consisting of 28 sites. The boundary waveguide is weakly coupled to the edge A site of the rhombic lattice. The inset shows a sketch of the system. Note that the boundary mode lies in the band gap above the flat band, and there is no lattice edge mode in the band gap. (b, c) Overlap of the normalized optical state with different eigenmodes of the system for two different g/J_1 values indicated in each figure.

nonlinearity, localization at the boundary waveguide is not destroyed, as evident by the overlap calculation in Fig. S3(b). As mentioned previously, flat band modes in our rhombic lattice are localized on the B and C sites of a unit cell with equal intensity and opposite phases. Hence, the flat band modes can not be excited by launching light at the boundary site coupled to the edge A site. Additionally, the formation of discrete breathers with oscillating intensity along the propagation distance does not occur in this case. At larger nonlinearity, relatively stronger detuning of the boundary site causes excitation of the lower dispersive band (Fig. S3(b)), and hence, light tunnels to the lattice.

-
- [1] Demetrios N Christodoulides, Falk Lederer, and Yaron Silberberg, “Discretizing light behaviour in linear and nonlinear waveguide lattices,” [Nature](#) **424**, 817–823 (2003).
 - [2] Ivan L. Garanovich, Stefano Longhi, Andrey A. Sukhorukov, and Yuri S. Kivshar, “Light propagation and localization in modulated photonic lattices and waveguides,” [Phys. Rep.](#) **518**, 1–79 (2012).
 - [3] S. Longhi, “Quantum-optical analogies using photonic structures,” [Laser & Photon. Rev.](#) **3**, 243–261 (2009).
 - [4] Tal Schwartz, Guy Bartal, Shmuel Fishman, and Mordechai Segev, “Transport and Anderson localization in disordered two-dimensional photonic lattices,” [Nature](#) **446**, 52–55 (2007).

- [5] Mordechai Segev, Yaron Silberberg, and Demetrios N Christodoulides, “Anderson localization of light,” [Nat. Photon. **7**, 197–204 \(2013\)](#).
- [6] D. N. Christodoulides and R. I. Joseph, “Discrete self-focusing in nonlinear arrays of coupled waveguides,” [Opt. Lett. **13**, 794–796 \(1988\)](#).
- [7] Mordechai Segev, Bruno Crosignani, Amnon Yariv, and Baruch Fischer, “Spatial solitons in photorefractive media,” [Phys. Rev. Lett. **68**, 923 \(1992\)](#).
- [8] H. S. Eisenberg, Yaron Silberberg, R Morandotti, A. R. Boyd, and J. S. Aitchison, “Discrete spatial optical solitons in waveguide arrays,” [Phys. Rev. Lett. **81**, 3383 \(1998\)](#).
- [9] Falk Lederer, George I Stegeman, Demetri N Christodoulides, Gaetano Assanto, Moti Segev, and Yaron Silberberg, “Discrete solitons in optics,” [Phys. Rep. **463**, 1–126 \(2008\)](#).
- [10] Sergej Flach and Charles R Willis, “Discrete breathers,” [Phys. Rep. **295**, 181–264 \(1998\)](#).
- [11] G Kopidakis and S Aubry, “Discrete breathers and delocalization in nonlinear disordered systems,” [Phys. Rev. Lett. **84**, 3236 \(2000\)](#).
- [12] Diana Mandelik, HS Eisenberg, Yaron Silberberg, R Morandotti, and JS Aitchison, “Observation of mutually trapped multiband optical breathers in waveguide arrays,” [Phys. Rev. Lett. **90**, 253902 \(2003\)](#).
- [13] Trideb Shit, Rishav Hui, Marco Di Liberto, Diptiman Sen, and Seababrata Mukherjee, “Intensity correlation measurement to simulate two-body bound states in the continuum and probe nonlinear discrete breathers,” [Phys. Rev. A **111**, 053515 \(2025\)](#).
- [14] F. Geniet and J. Leon, “Energy transmission in the forbidden band gap of a nonlinear chain,” [Phys. Rev. Lett. **89**, 134102 \(2002\)](#).
- [15] Ramaz Khomeriki, “Nonlinear band gap transmission in optical waveguide arrays,” [Phys. Rev. Lett. **92**, 063905 \(2004\)](#).
- [16] H Susanto and N Karjanto, “Calculated threshold of supratransmission phenomena in waveguide arrays with saturable nonlinearity,” [J. Nonlinear Opt. Phys. & Mat. **17**, 159–165 \(2008\)](#).
- [17] AB Togueu Motcheyo, JD Tchinang Tchameu, M Siewe Siewe, and Clément Tchawoua, “Homoclinic nonlinear band gap transmission threshold in discrete optical waveguide arrays,” [Communications in Nonlinear Science and Numerical Simulation **50**, 29–34 \(2017\)](#).
- [18] P. Zakharov, “The effect of nonlinear supratransmission in discrete structures: A review,” [Comput. Res. Model **15**, 599–617 \(2023\)](#).

- [19] H Susanto, N Lazarides, and I Kourakis, “Surge of power transmission in flat and nearly flat band lattices,” [Phys. Rev. E **108**, L052201 \(2023\)](#).
- [20] J.E. Macías-Díaz and A. Puri, “An application of nonlinear supratransmission to the propagation of binary signals in weakly damped, mechanical systems of coupled oscillators,” [Phys. Lett. A **366**, 447–450 \(2007\)](#).
- [21] Alain Bertrand Togueu Motcheyo and J. Macías-Díaz, “Nonlinear bandgap transmission with zero frequency in a cross-stitch lattice,” [Chaos Solitons and Fractals **170**, 113349 \(2023\)](#).
- [22] H Tasaki, “Hubbard model and the origin of ferromagnetism,” [Eur. Phys. J. B **64**, 365–372 \(2008\)](#).
- [23] Daniel Leykam and Sergej Flach, “Perspective: photonic flatbands,” [APL Photon. **3**, 070901 \(2018\)](#).
- [24] Seababrata Mukherjee, Alexander Spracklen, Debaditya Choudhury, Nathan Goldman, Patrik Öhberg, Erika Andersson, and Robert R. Thomson, “Observation of a localized flat-band state in a photonic Lieb lattice,” [Phys. Rev. Lett. **114**, 245504 \(2015\)](#).
- [25] Rodrigo A Vicencio, Camilo Cantillano, Luis Morales-Inostroza, Bastián Real, Cristian Mejía-Cortés, Steffen Weimann, Alexander Szameit, and Mario I Molina, “Observation of localized states in Lieb photonic lattices,” [Phys. Rev. Lett. **114**, 245503 \(2015\)](#).
- [26] Seababrata Mukherjee and Robert R. Thomson, “Observation of localized flat-band modes in a quasi-one-dimensional photonic rhombic lattice,” [Opt. Lett. **40**, 5443–5446 \(2015\)](#).
- [27] D Guzmán-Silva, C Mejía-Cortés, M A Bandres, M C Rechtsman, S Weimann, S Nolte, M Segev, A Szameit, and R A Vicencio, “Experimental observation of bulk and edge transport in photonic Lieb lattices,” [New J. Phys. **16**, 063061 \(2014\)](#).
- [28] Seababrata Mukherjee, Marco Di Liberto, Patrik Öhberg, Robert R Thomson, and Nathan Goldman, “Experimental observation of Aharonov-Bohm cages in photonic lattices,” [Phys. Rev. Lett. **121**, 075502 \(2018\)](#).
- [29] Shiqiang Xia, Yi Hu, Daohong Song, Yuanyuan Zong, Liqin Tang, and Zhigang Chen, “Demonstration of flat-band image transmission in optically induced Lieb photonic lattices,” [Opt. Lett. **41**, 1435–1438 \(2016\)](#).
- [30] Shintaro Taie, Hideki Ozawa, Tomohiro Ichinose, Takuei Nishio, Shuta Nakajima, and Yoshiro Takahashi, “Coherent driving and freezing of bosonic matter wave in an optical Lieb lattice,” [Science Advances **1**, e1500854 \(2015\)](#).

- [31] Chao Zeng, Yue-Ran Shi, Yi-Yi Mao, Fei-Fei Wu, Yan-Jun Xie, Tao Yuan, Wei Zhang, Han-Ning Dai, Yu-Ao Chen, and Jian-Wei Pan, “Transition from flat-band localization to Anderson localization in a one-dimensional tasaki lattice,” [Phys. Rev. Lett. **132**, 063401 \(2024\)](#).
- [32] Sebastian A Schulz, Jeremy Upham, Liam O’Faolain, and Robert W Boyd, “Photonic crystal slow light waveguides in a kagome lattice,” [Opt. Lett. **42**, 3243–3246 \(2017\)](#).
- [33] Govind P Agrawal, “Nonlinear fiber optics,” in *Nonlinear Science at the Dawn of the 21st Century* (Springer, 2000).
- [34] M. Ams, G. D. Marshall, D. J. Spence, and M. J. Withford, “Slit beam shaping method for femtosecond laser direct-write fabrication of symmetric waveguides in bulk glasses,” [Opt. Express **13**, 5676–5681 \(2005\)](#).
- [35] K. M. Davis, K. Miura, N. Sugimoto, and K. Hirao, “Writing waveguides in glass with a femtosecond laser,” [Opt. Lett. **21**, 1729–1731 \(1996\)](#).
- [36] SR Friberg, Y Silberberg, MKr Oliver, MJ Andrejco, MA Saifi, and PW Smith, “Ultrafast all-optical switching in a dual-core fiber nonlinear coupler,” [Appl. Phys. Lett. **51**, 1135–1137 \(1987\)](#).
- [37] Giorgos Demetriou, Daniel W Hewak, Andrea Ravagli, Chris Craig, and Ajoy Kar, “Nonlinear refractive index of ultrafast laser inscribed waveguides in gallium lanthanum sulphide,” [Appl. Optics **56**, 5407–5411 \(2017\)](#).
- [38] Gayathry Rajeevan and Sebabrata Mukherjee, “Nonlinear switch and spatial lattice solitons of photonic s–p orbitals,” [Opt. Lett. **50**, 297–300 \(2025\)](#).
- [39] Yuan Cao, Valla Fatemi, Shiang Fang, Kenji Watanabe, Takashi Taniguchi, Efthimios Kaxiras, and Pablo Jarillo-Herrero, “Unconventional superconductivity in magic-angle graphene superlattices,” [Nature **556**, 43–50 \(2018\)](#).
- [40] Marco Di Liberto, Sebabrata Mukherjee, and Nathan Goldman, “Nonlinear dynamics of Aharonov-Bohm cages,” [Phys. Rev. A **100**, 043829 \(2019\)](#).
- [41] Goran Gligorić, Petra P Beličev, Daniel Leykam, and Aleksandra Maluckov, “Nonlinear symmetry breaking of Aharonov-Bohm cages,” [Phys. Rev. A **99**, 013826 \(2019\)](#).
- [42] V Goblot, B Rauer, F Vicentini, A Le Boité, Elisabeth Galopin, A Lemaître, L Le Gratiet, A Harouri, I Sagnes, S Ravets, *et al.*, “Nonlinear polariton fluids in a flatband reveal discrete gap solitons,” [Phys. Rev. Lett. **123**, 113901 \(2019\)](#).

- [43] G Pelegrí, AM Marques, V Ahufinger, J Mompart, and RG Dias, “Interaction-induced topological properties of two bosons in flat-band systems,” [Phys. Rev. Res. **2**, 033267 \(2020\)](#).